Next Materials 9 (2025) 101290

Contents lists available at ScienceDirect

Next Materials

journal homepage: www.sciencedirect.com/journal/next-materials

Research article

Dual-function Cameroonian clay-supported ZnO and TiO_2 photocatalysts for ibuprofen mineralization and bacterial inactivation

Marlène Huguette Tsaffo Mbognou [a,b,c], Stéphanie D. Lambert [a], Antoine Farcy [a], Hela Rekik [d], Steven C.N. Wouamba [e,f], Emmanuel Djoufac Woumfo [b], Julien G. Mahy [a,*]

[a] Department of Chemical Engineering – Nanomaterials, Catalysis & Electrochemistry, University of Liège, B6a, Quartier Agora, Allée du six Août 11, Liège 4000, Belgium
[b] Laboratoire de Physico-chimie des matériaux minéraux, University of Yaounde, I, 337, Yaounde, Cameroon
[c] Institute of Geological and Mining Research (IRGM), Yaounde 4110, Cameroon
[d] Institut National de la Recherche Scientifique (INRS), Centre-Eau Terre Environnement, Université du Québec, 490, Rue de la Couronne, Québec, QC G1K 9A9, Canada
[e] Department of Chemistry, Higher Teacher Training College, University of Yaounde I, P.O. Box 47, SPO, Yaounde, Cameroon
[f] Université de Montpellier, INRAE, Montpellier SupAgro, Montpellier 34000, France

ARTICLE INFO

Keywords:
Ibuprofen
Photocatalysis
ZnO/TiO_2-doped clay
Mineralization
Antibacterial activity
Wastewater treatment

ABSTRACT

The increasing presence of pharmaceuticals, such as ibuprofen, in wastewater poses significant environmental and public health challenges, particularly in developing regions. In this study, we developed photocatalytic materials by doping natural Cameroonian clay with ZnO and TiO_2 to achieve efficient ibuprofen mineralization and bacterial inactivation under ultra-violet (UV) light. Characterization confirmed the successful integration of semiconductors into the clay matrix, which enhanced the surface area to 325 m^2/g for TiO_2-based composites. Under UVA irradiation (1.2 mW/cm^2), the Cu-doped TiO_2/clay composite achieved 48 % ibuprofen mineralization, measured by Total Organic Carbon (TOC) reduction, within 4 h, while ZnO-based composites reached up to 23 % under similar conditions. Antibacterial tests demonstrated complete inhibition of Shigella spp., total coliforms, and faecal streptococci at a catalyst dosage of 1 g/L under UVA, highlighting the dual functionality of the materials. These low-cost, locally sourced photocatalysts show promise for integrated pharmaceutical and microbial removal in decentralized wastewater treatment systems, offering a sustainable solution for water purification in resource-limited settings.

1. Introduction

Over the past two decades, numerous studies have reported the presence of harmful substances in environmental matrices such as sewage, surface and groundwater, and even drinking water [1–3]. According to the World Health Organization (WHO), approximately 10 % of the global population consumes food irrigated with untreated wastewater [4]. This widespread reuse of contaminated water contributes to the spread of waterborne diseases such as amoebiasis, affecting both industry workers and local populations, regardless of age, gender, or social status [1].

In many African countries, particularly in Cameroon, over 90 % of human waste is managed through non-centralized systems and is often discharged directly into the environment without proper treatment [3]. Such practices have severe implications for both human health and ecosystems, as fecal sludge is often rich in pathogenic indicator bacteria (E. coli, Shigella, fecal streptococci) and contains high levels of pharmaceutical residues.

Among these contaminants, ibuprofen, a widely used non-steroidal anti-inflammatory drug, has been frequently detected in the effluents of wastewater treatment plants and in surface waters at concentrations ranging from $ng{\cdot}L^{-1}$ to $\mu g{\cdot}L^{-1}$ [5,6]. It poses ecotoxicological risks to aquatic organisms and potential health concerns to humans [7–9]. Conventional wastewater treatment technologies often fail to remove such micropollutants effectively. Consequently, tertiary treatment approaches, particularly advanced oxidation processes (AOPs), have emerged as promising alternatives for degrading and mineralizing persistent organic pollutants, including pharmaceuticals and pathogenic microorganisms. AOPs operate through the generation of highly reactive and non-selective oxidizing species, primarily hydroxyl radicals ($^{\bullet}OH$), which can break down most organic compounds present in water [10–15].

* Corresponding author.
E-mail address: julien.mahy@uliege.be (J.G. Mahy).

https://doi.org/10.1016/j.nxmate.2025.101290
Received 5 August 2025; Received in revised form 27 September 2025; Accepted 30 September 2025
Available online 3 October 2025
2949-8228/© 2025 The Authors. Published by Elsevier Ltd. This is an open access article under the CC BY-NC license (http://creativecommons.org/licenses/by-nc/4.0/).

Recent advancements in AOPs have emphasized the development of clay-supported semiconductor composites for enhanced degradation of pharmaceuticals and dyes, underscoring the potential for sustainable water treatment. For instance, Trigueiro et al. [16] synthesized a ZnO-alginate-hectorite nanocomposite achieving 65.55 % furosemide and 93 % ciprofloxacin removal under UV light within 120 min, with a band gap of 3.27 eV and predominant defects like zinc (V_{Zn} = 35.64 %) and oxygen vacancies (V_{O+} = 56.05 %, V_O = 8.31 %). Similarly, Y-doped ZnO on alginate-hectorite supports provided over 90 % degradation of direct blue 71 and 79 % of reactive black 5 in 120 min, driven by hydroxyl radicals [17]. Albuquerque et al. [18] reported a RuO_2@ZnO-alginate-halloysite composite with band gaps from 3.281 to 3.252 eV, degrading 82.53 % ciprofloxacin and 68.68 % eosin yellow under UV, with superoxide (•O_2^-) and hydroxyl (•OH) as key species. Trigueiro et al. [19] developed CuO-TiO_2-saponite nanocomposites achieving 83 % bromocresol green discoloration in 150 min via hydroxyl and superoxide radicals. Feitosa et al. [20] used Ce-doped TiO_2-sepiolite for 70.45 % tetracycline inactivation (35.11 % photocatalysis), primarily via holes (h^+). Hamarawf et al. [21] introduced a Fe^{2+}/Fe^{3+} mixed-valency porous coordination polymer with antibacterial activity (MIC 0.4 mg/mL against S. aureus, E. coli, P. aeruginosa) and 99.16 % rhodamine B degradation in 70 min via photo-Fenton, involving •OH (79.2 %), O_2•$^-$ (20.7 %), and h^+ (16.4 %). Specifically for ibuprofen, Aziz et al. [22] employed a TiO_2-coated falling film reactor under UVA, identifying low mineralization with by-products like formic and acetic acids. Soares et al. [23] showed pH-dependent Co-doped ZnO achieving up to 20 % ibuprofen degradation under UV with H_2O_2. These studies highlight the efficacy of hybrid materials but reveal gaps in using underexplored local clays like Cameroonian smectite for ibuprofen photodegradation, which this work addresses through low-cost, dual-functional ZnO/TiO_2-doped composites.

Photocatalysis, one of the most widely studied AOPs, relies on the activation of semiconductor materials such as titanium dioxide (TiO_2) or zinc oxide (ZnO) under UV irradiation [10,24,25]. These photocatalysts generate photo-induced electron-hole pairs (e^-/h^+), which in turn initiate the formation of reactive oxygen species. For instance, Méndez-Arriaga et al. [26] successfully demonstrated the photocatalytic degradation of highly concentrated ibuprofen (200 mg·L^{-1}) using TiO_2 in suspension under simulated solar light. Walczak et al. [5] showed the effective degradation of ibuprofen with TiO_2 doped with carbon nanotube up to 20 % in 1 h UV–visible exposition. While effective, the use of photocatalysts in suspension suffers from practical limitations such as aggregation, post-treatment recovery issues, and low adsorption capacity [5].

To overcome these limitations, research has increasingly focused on the development of hybrid materials combining photocatalysts with natural or engineered supports. In this context, clay minerals, particularly smectites, offer an attractive platform due to their low cost, chemical and mechanical stability, large surface area, high cation exchange capacity, and environmental compatibility [27–29]. In the African context, local clays, including those from Cameroon, remain largely underexplored despite their potential as adsorbents or catalysts. Promising results have been reported for the adsorption or degradation of dyes and volatile organic compounds, including green malachite and similar pollutants [30,31]. Nevertheless, applications targeting pharmaceuticals remain scarce and, to our knowledge, no published studies have yet investigated the photochemical degradation of ibuprofen using visible or UVA light on Cameroonian clays modified with photocatalysts.

Furthermore, in the search for multifunctional materials, the integration of antimicrobial activity into photocatalytic systems is gaining interest, especially in regions where waterborne pathogens pose a major health risk. The incorporation of metal ions (e.g., Cu^+, Zn^{2+}) into clay structures has been shown to enhance antibacterial effects, which could offer a dual action strategy: the degradation of pharmaceutical residues and the disinfection of contaminated water [32,33].

In this study, we synthesized and characterized composite photocatalysts based on natural Cameroonian smectite clay, doped with TiO_2 or ZnO nanoparticles, with or without ion-exchange modifications using Na^+, Zn^{2+}, or Cu^+ cations. Comprehensive analyses, including X-ray diffraction (XRD), scanning electron microscopy (SEM), and nitrogen adsorption-desorption, confirmed the successful integration of semiconductors into the clay matrix, enhancing surface area for composites and optimizing particle dispersion. We evaluated their performance for the photocatalytic degradation of ibuprofen under UVA (1.2 mW/cm^2) and UV-Visible (UV-Vis) irradiation, with mineralization efficiency quantified via Total Organic Carbon (TOC) analysis. This approach provides a rigorous assessment of complete pollutant breakdown into inorganic end-products, surpassing the limitations of UV-Vis spectroscopy alone and addressing a gap in similar studies where partial degradation is often reported.

In parallel, the antimicrobial properties of these materials were examined to assess their potential for simultaneous pharmaceutical removal and microbial disinfection. Antibacterial tests targeted waterborne pathogens, including Shigella spp., total coliforms, and faecal streptococci, under controlled UVA conditions. We hypothesize that the incorporation of TiO_2 or ZnO, combined with cationic modifications, will enhance ibuprofen mineralization by up to 50 % (based on preliminary TOC data) and achieve complete inhibition of these pathogens at a catalyst dosage of 1 g/L within 4 h, driven by improved surface charge, porosity, and reactive oxygen species (ROS) generation. This work proposes a multifunctional strategy, using locally sourced Cameroonian clay to develop low-cost, eco-compatible photocatalysts that integrate adsorption, photocatalysis, and antibacterial activity. By targeting this underexplored research niche, the study contributes to an innovative solution for sustainable water treatment technologies tailored to the needs of developing regions, particularly in the African context.

2. Materials and methods

2.1. Clay description and modification

A natural smectite clay was extracted from Bakotcha, in the western region of Cameroon (details in [13]). After drying to constant weight, the clay was modified via interlayer cation exchange with Cu^{2+} and Zn^{2+} ions, as well as homoionization with Na^+ ions.

2.1.1. Sodium Ion Insertion

The detailed protocol is given in [31] and summarized here. The following reagents were used: distilled water, sodium chloride (≥99.5 %, Fisher BioReagents), silver nitrate (99 %, ultrapure, Laboratorium Discounter), and clay powder (>160 μm). Sodium homoionization was performed to replace all exchangeable cations with Na^+: 100 g of clay was stirred in 1 M NaCl solution for 72 h. After drying at 100 °C for 24 h, the material was stirred again in NaCl for 4 h to promote cation exchange.

After settling, the supernatant was discarded and the solid was redispersed in a fresh NaCl solution. This step was repeated four times. The clay was then washed with distilled water until no chloride ions were detected via the silver nitrate test. A negative result (no precipitate) confirmed successful washing. The Na^+-homoionic clay was dried at 100 °C overnight.

2.1.2. Zinc ion insertion

The detailed protocol is given in [13] and summarized here. This treatment allowed incorporation of Zn^{2+} without altering the clay structure. The reagents used were zinc(II) chloride (≥97.0 %, Laboratorium Discounter), silver nitrate (99 %, ultrapure), clay powder (>160 μm), and distilled water. 50 g of clay was stirred in 0.1 M $ZnCl_2$ for 4 h. After settling for 2 h, the supernatant was discarded and replaced with fresh $ZnCl_2$ solution. The process was repeated twice. Washing continued until a negative silver nitrate test confirmed the removal of

excess Cl^-. The Zn^{2+}-homoionic clay was then dried overnight at 100 °C.

2.1.3. Copper ion insertion

The detailed protocol is given in [13] and summarized here. The reagents were copper(II) sulfate pentahydrate (≥98.0 %, Sigma-Aldrich), barium sulfate (99 %, Sigma-Aldrich), clay powder (>160 μm), and distilled water. 50 g of clay was stirred in 0.1 M $CuSO_4$ for 4 h, allowed to settle for 2 h and then treated with fresh $CuSO_4$ solution. This process was repeated twice. The material was washed with distilled water until no SO_4^{2-} ions were detected using the barium precipitation test. The Cu^{2+}-homoionic clay was then dried at 100 °C overnight.

2.2. Synthesis of pure TiO_2 and ZnO photocatalysts

2.2.1. ZnO powder

The sol-gel method by Benhebal et al. [34] was used. Reagents included absolute ethanol (ACS grade), oxalic acid dihydrate (99 %), and zinc acetate dihydrate (98 %) from BIOCHEM Chemopharma (France). 10.98 g of zinc acetate was dissolved in 300 mL ethanol at 60 °C. Separately, 12.6 g of oxalic acid was dissolved in 200 mL ethanol at the same temperature. The oxalic acid solution was slowly added to the zinc solution while stirring for 90 min at 50 °C. The gel was dried at 80 °C for 24 h and calcined at 400 °C for 4 h, resulting in a white ZnO powder.

2.2.2. TiO_2 powder

The sol-gel method by Mahy et al. [35] was followed. Reagents: isopropanol (99.5 %, Acros), nitric acid (65 %, Merck), titanium(IV) tetraisopropoxide (TTIP ≥ 97 %, Sigma-Aldrich), and distilled water.

250 mL of distilled water was acidified to pH 1 with HNO_3. Then, 15 mL TTIP and 15 mL isopropanol were mixed and stirred for 30 min at room temperature. This solution was added dropwise to the acidified water under continuous stirring and heated to 80 °C for 4 h. A blue sol formed. After drying under airflow for 10 h, the xerogel was obtained. It was then dried at 100 °C for 1 h, yielding a yellowish-white TiO_2 powder.

2.3. Synthesis of clay/photocatalyst composites

2.3.1. Clay/ZnO composites

Following the ZnO synthesis protocol, 10 g of clay was added during the oxalic acid addition step. The mixture was stirred for 90 min at 50 °C. After gelation and drying at 80 °C for 24 h, the composite was calcined at 400 °C for 4 h. The final material appeared light grey. The samples are called A-X/ZnO with X standing for a specific cation (Cu, Zn or Na). The raw clay modified with ZnO is called A/ZnO.

2.3.2. Clay/TiO_2 composites

Following the TiO_2 synthesis method, 10 g of clay was added to the blue sol and stirred for 2 h. The mixture was dried for 24 h to obtain the clay/TiO_2 hybrid material. The samples are named similarly to the ZnO series, replacing ZnO with TiO_2.

2.4. Characterization techniques

The apparent density was measured using a Micromeritics AccuPyc 1330 helium pycnometer at 20 °C and 18 psi. Three replicates per sample were performed and average values were reported with < 1 % standard deviation.

Specific surface area was determined by nitrogen adsorption–desorption isotherms at 77 K using a Micromeritics ASAP 2420 instrument.

SEM imaging (15 kV) was performed using a Bruker TESCAN CLARA. Samples were sonicated in acetone, deposited on slides, and gold-coated before observation.

Zeta potential and hydrodynamic diameter were measured by dynamic light scattering (DLS) using a Beckman Coulter DelsaNano C.

The point of zero charge (PZC) of each sample was determined using the method described by [36]. Eleven vials were prepared, each containing 10 mL of Milli-Q water. The initial pH of each vial was adjusted using diluted HCl or NaOH to cover a pH range from 2 to 10, with an increment of 1 pH unit between successive vials. An equal volume of the sample suspension was then added to each vial. The amount of sample added was calculated to achieve a surface concentration of 1000 $m^2 \cdot L^{-1}$, corresponding to a total surface area of 10 m^2 in 10 mL, depending on the specific surface area of the material. The vials were then shaken for 1 h to allow equilibration. After this time, the final pH of each solution was measured. A graph was plotted comparing the final and initial pH values, and the PZC was determined as the pH value at which the curve reaches a plateau, as described by [36]. All pH measurements were carried out using a Systronics μ 362 pHmeter (India).

ICP–AES (ICAP 6500 THERMO Scientific) was used to determine elemental composition [37]. HF digestion was used for mineralization [13,37].

XRD analysis was performed using a Bruker D8 Twin-Twin diffractometer with Cu-Kα radiation.

Similar comprehensive characterization approaches, including XRD, SEM-EDS, BET, and FTIR, have been employed in [38]. This reference underscores the importance of multi-technique analysis in validating catalyst efficacy for AOPs targeting pharmaceuticals.

2.5. Analytical methods

2.5.1. Photocatalytic activity

The photocatalytic activity of the synthesized materials was evaluated by monitoring the degradation of ibuprofen (IBU) under UV irradiation. The experiments were performed using 2 types of UV lamps: one emitting at 365 nm (Osram F18W/BLB-T8, 1.2 mW/cm^2) and one halogen lamp (with a continuous spectrum from 300 to 800 nm (300 W, 220 V), 78 mW/cm^2 with 77 mW/cm^2 in the visible range) placed in a irradiation chamber [39], maintaining a constant distance of 20 cm between the light source and the sample surface.

For each material, 50 mL of an aqueous ibuprofen solution (initial concentration: 52 mg/L) was placed in a flat Petri dish with a diameter of 8.5 cm. All tests were conducted under magnetic stirring in the dark for 30 min prior to irradiation, to ensure adsorption–desorption equilibrium. After this equilibration period, the samples were irradiated for up to 4 h. The reactor temperature was maintained at 25 ± 2 °C.

Three independent replicates were performed for each material. Control experiments were conducted under the same conditions and also in the dark using (i) raw clay, (ii) TiO_2 or ZnO alone, and (iii) the ibuprofen solution without any added material to distinguish between adsorption, photolysis, and photocatalytic degradation.

At regular time intervals (typically every 2 h), 20 mL aliquots were withdrawn, filtered through 0.45 μm membranes, and stored at 4 °C prior to analysis. The degradation of ibuprofen was monitored using Total Organic Carbon (TOC) analysis. TOC was performed using a Shimadzu TOC-L analyzer equipped with an autosampler and a high-sensitivity catalyst. TOC reduction was used to assess the mineralization efficiency of each material.

All measurements were conducted in triplicate, and the mean values are reported with standard deviations below 5 %.

For the two best composite samples, a kinetic study is performed under UVA light. From [40], IBU degradation can be described by the following equation:

$$C = C_0 e^{\left(-k\frac{m}{V_0}t\right)} \quad (1)$$

Where C is the concentration of the pollutant, C_0 is the initial concentration of the pollutant, k is the kinetic constant, m is the mass of the catalyst, V_0 is the initial solution volume, and t is the time.

By plotting -ln(C/C$_0$) as a function of time t, the constant reaction rate k, can be determined [41].

The amount of metal ion released during photocatalytic experiments under UVA after 4 h was also measured for TiO_2, A/TiO_2, ZnO and A-Cu/ZnO samples. After 4 h of photocatalytic experiments under UVA light, the water medium is filtered with syringe filter (polypropylene, 13 mm diameter, 0.2 µm pore size, Whatman™, VWR) and the metal ion (Ti, Zn, Cu) content in the filtrate is measured by ICP-AES.

2.5.2. Scavenger experiments

Ammonium oxalate (AO, 5 mM), isopropanol (ISOP, 5 mM), and p-benzoquinone (PB, 0.5 mM) are used as, respectively, hole, hydroxyl radical and superoxide scavenger in ibuprofen aqueous solution filled with the two best composite samples (A/ZnO and A-Cu/TiO_2) with a photocatalyst concentration of 1 g/L, inspired by [40,42,43]. Measurements are performed after 4 h (under UVA light) using TOC measurements previously calibrated with the scavengers.

2.5.3. Antibacterial assay

Wastewater was collected from the wastewater treatment plant « Cité verte » Yaoundé-Cameroun and used for the antibacterial experiments. 50 mL of this wastewater was stirred with the samples (with a concentration of 0.5, 1, or 10 g/L) under UVA illumination (365 nm) for 4 h at a control temperature of 25 °C. Then the bacterial content (3 types: total coliforms, faecal coliforms, and faecal streptococci) was evaluated with the protocol below. Control experiments were made without samples both with and without illumination to highlight the effect of the materials on the bacteria and also with the materials and no light.

a) Bacterial Strains analyzed

The culture media used were as follows:

XLD agar (Xylose-Lysine-Deoxycholate agar): a moderately selective and differential medium for the isolation and differentiation of Gram-negative enteric pathogens. It was specifically used for the identification of Salmonella and Shigella species.

Endo agar: a slightly selective and differential culture medium for the detection of coliforms and other enteric bacteria. It was primarily used to identify Escherichia coli and to enumerate total and faecal coliforms.

BEA agar (Bile Esculin Agar): a selective and differential medium used to detect group D Enterococci and Streptococcus. Only colonies forming black precipitates were counted.

b) Bacteriological Analysis

The bacteriological analysis focused on indicator organisms of microbial contamination, namely: total coliforms, faecal coliforms, and faecal streptococci.

Colonies were enumerated using two complementary techniques for data validation: surface plating and flooding on nutrient agar. Incubation was performed at 37 °C for 24 h for total and faecal coliforms, and 48 h for faecal streptococci.

Mueller-Hinton Dilution Method

The antibacterial activity of the hybrid materials was also assessed using the dilution method on Mueller–Hinton agar. In this assay, bacteria were cultured in the presence of increasing concentrations of the hybrid material (0.5 g·L^{-1}, 1 g·L^{-1}, and 10 g·L^{-1}). After incubation, the presence or absence of bacterial colonies was macroscopically examined to evaluate bacterial growth inhibition.

Sterilized distilled water (autoclaved at 121 °C for 15 min) was used as a diluent, with serial dilutions being performed up to 1:100,000 for highly contaminated samples. Three agar plates per dilution were inoculated using both surface plating and flooding methods. Colony counts were performed after incubation (37 °C for 24 h for total coliforms and Salmonella/Shigella; 37 °C for 48 h for faecal streptococci), and the results were corrected based on the dilution factors.

Results are expressed as log colony-forming units per milliliter (log (CFU·mL^{-1})) according to established procedures [44]. Colonies were counted only on plates with 15–300 colonies. If all plates contained fewer than 15 colonies, all observed colonies were counted, considering the total inoculated volume.

3. Results

3.1. Composition and crystallinity of samples

The elemental composition of the synthesized samples was determined by inductively coupled plasma atomic emission spectroscopy (ICP-AES) and is reported in Table 1. As expected, the raw clay is primarily composed of aluminum and silicon, with an Al/Si ratio close to 2, which is characteristic of smectite-type clays [13]. Upon incorporation of metal ions (Cu, Na, or Zn), a corresponding increase in the concentration of these elements is clearly observed, confirming the success of the ion-exchange process.

For the composite materials, the incorporation of 30 wt% photocatalyst (either TiO_2 or ZnO) was achieved as intended, according to the measured compositions. These values are consistent with similar materials reported in the literature [13], supporting the reproducibility and reliability of the synthesis route employed.

The crystalline structure of the samples was analyzed by X-ray diffraction (XRD), and representative diffractograms are presented in Fig. 1. The raw clay exhibits a complex mineralogical composition, including phases such as augite, cristobalite, montmorillonite, illite, kaolinite, feldspar, and talc. These phases remain identifiable in the ion-exchanged clays, indicating that the structural integrity of the clay matrix is largely preserved after modification.

The diffractograms of the pure ZnO and TiO_2 photocatalysts show diffraction peaks corresponding to the wurtzite structure for ZnO and a mixture of anatase and brookite for TiO_2. Accordingly, these crystalline phases are also observed in the composite samples, confirming the successful integration of the photocatalyst without significant alteration of its crystal structure. These findings are consistent with those reported in our previous study using similar preparation protocols [13].

Overall, the XRD and ICP-AES results jointly demonstrate that the synthesis procedure yields stable and well-defined clay-based composite materials with preserved crystalline properties and controlled photocatalyst loading.

3.2. Textures and morphology of samples

The textural properties and colloidal behavior of the prepared composites were assessed through BET surface area analysis, pore volume (V_p), apparent density (ρ_{app}), zeta potential measurements, and dynamic light scattering (DLS). These parameters are summarized in Table 2.

The pristine clay exhibited a modest surface area (45 m^2/g) and low

Table 1
Sample compositions by ICP-AES.

	Al	Si	Fe	Cu	TiO_2	ZnO
	wt%	wt%	wt%	wt%	wt%	wt%
Raw clay	10.1	20.9	3.7	< 0.1	< 0.1	< 0.1
A/ZnO	5.2	9.2	1.6	< 0.1	< 0.1	28.1
A-Cu/ZnO	6.4	11.6	1.8	0.4	< 0.1	30.3
A-Na/ZnO	5.9	11.7	1.7	< 0.1	< 0.1	29.6
A-Zn/ZnO	6.2	12.1	1.8	< 0.1	< 0.1	28.5
A/ TiO_2	5.7	10.2	1.6	< 0.01	28.8	< 0.1
A-Cu/ TiO_2	5.9	11.6	1.2	0.3	27.6	< 0.1
A-Na/ TiO_2	5.8	11.2	1.4	< 0.01	29.1	< 0.1
A-Zn/ TiO_2	6.1	11.6	1.5	< 0.01	28.6	0.4

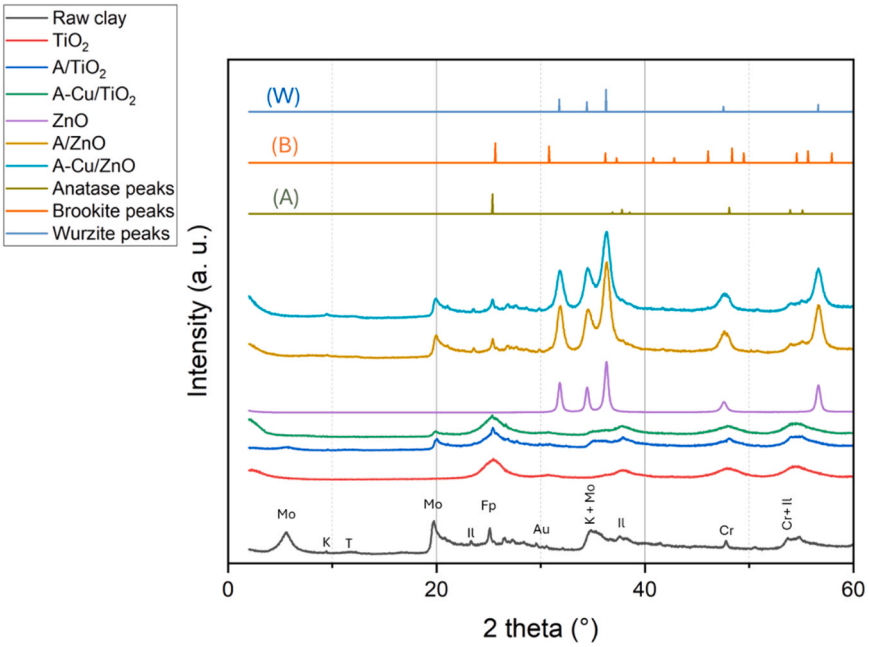

Fig. 1. XRD patterns of samples: raw clay, TiO_2, A/TiO_2, A-Cu/TiO_2, ZnO, A/ZnO, A-Cu/ZnO. Reference peak positions of the different phases of the raw clay are indicated directly on the diffractogram by the following letters: (A) anatase, (B) brookite, (Z) wurzite, (Mo) montmorillonite, (T) talc, (K) kaolinite, (Il) illite, (Fp) feldspar, (Au) augite, and (Cr) cristobalite. The positions are not indicated on the composite materials to avoid overloading the figure. The reference patterns of anatase ((A) from JCPDS 71–1167) [45], brookite ((B) from JCPDS 29–1360) [45] and wurzite ((W) from JCPDS 36–1451) [46] are represented in the range 2–60°.

Table 2
Physico-chemical properties of samples.

Sample	ρ_{app} (g/cm^3) ± 0.01	S_{BET} (m^2/g) ± 5	V_P (cm^3/g) ± 0.01	Zeta potential (mV) ± 0.01	pH of zeta potential (-) ± 0.1	DLS (nm) ± 10	PZC (-) ± 0.1
Raw clay	2.29	45	0.07	−10.94	5.4	4860	5.5
ZnO	6.23	30	0.14	14.61	7.1	6088	7.2
A-ZnO	2.64	125	0.44	2.20	5.3	2786	5.2
A-Cu-ZnO	3.09	50	0.21	12.22	7.2	4318	7.4
A-Na-ZnO	3.15	55	0.25	13.24	7.3	3503	7.4
A-Zn-ZnO	3.19	50	0.18	13.24	7.2	1612	7.1
TiO_2	2.98	180	0.12	24.51	2.7	1554	3
A-TiO_2	2.90	325	0.23	2.50	3.2	10648	3.1
A-Cu-TiO_2	2.56	240	0.15	−3.27	3.1	6451	3.3
A-Na-TiO_2	2.48	110	0.11	−12.99	4.0	3761	4.1
A-Zn-TiO_2	2.48	130	0.14	−4.15	4.3	1461	4.1

ρ_{app}: apparent density measured by helium pycnometry; S_{BET}: specific surface area determined by BET method; V_p: specific liquid volume adsorbed at saturation pressure of nitrogen; D_{DLS}: hydrodynamic diameter of TiO_2 particles aggregates measured by DLS; Zeta potential analysis and pH at different zeta potential; PZC: point of zero charge.

pore volume (0.07 cm^3/g), consistent with the compact structure of untreated layered silicates. Upon modification with ZnO or TiO_2, the surface area and porosity were significantly altered depending on the nature of the inserted ion and photocatalyst.

Among ZnO-based composites, the A/ZnO material showed a considerable increase in specific surface area (125 m^2/g) and pore volume (0.44 cm^3/g), suggesting that ZnO nanoparticles were well-dispersed within the clay matrix, creating additional porosity. In contrast, ion-inserted ZnO composites such as A-Cu/ZnO, A-Na/ZnO, and A-Zn/ZnO displayed reduced surface areas (50–55 m^2/g) and moderate pore volumes (0.18–0.25 cm^3/g), likely due to partial pore blocking or aggregation of ZnO particles in the presence of the inserted metal ions. Notably, the apparent density increased significantly in these doped samples (above 3.0 g/cm^3), indicating a more compact or denser composite structure.

The bare ZnO material had a low surface area (30 m^2/g), highlighting the beneficial role of the clay as a structuring and dispersing matrix for photocatalysts. Moreover, the DLS data suggest that ZnO formed relatively large aggregates (hydrodynamic diameters above 1600 nm), especially in A-Zn/ZnO, possibly limiting accessibility to active sites.

TiO_2-based composites exhibited distinct behavior. The A/TiO_2 sample demonstrated a remarkably high surface area (325 m^2/g), which is significantly higher than both the pristine clay and the pristine TiO_2 (180 m^2/g). This suggests that TiO_2 was homogeneously distributed over or within the clay layers, contributing to extensive mesoporous features. However, the inclusion of dopants (Cu, Na, Zn) generally led to surface area reductions (110–240 m^2/g), in line with a potential pore-blocking effect or formation of larger aggregates. For instance, A-Cu/TiO_2 and A-Zn/TiO_2 retained relatively high values (240 and 130 m^2/g, respectively), while A-Na/TiO_2 dropped to 110 m^2/g, possibly reflecting a higher degree of TiO_2 particle clustering or coverage by exchanged ions.

In terms of particle aggregation, the TiO_2-based composites presented larger DLS values than their ZnO counterparts, with A/TiO_2 reaching 10648 nm, suggesting the formation of large agglomerates in suspension. This behavior may stem from the higher surface energy and propensity for aggregation of anatase/brookite nanoparticles.

Overall, these results highlight that the presence of clay not only acts as a structural support but also significantly modifies the textural features of the photocatalysts. The ion-exchange step appears to modulate porosity and particle dispersion, impacting potential photocatalytic and antimicrobial performances.

Scanning Electron Microscopy (SEM) was employed to investigate the surface morphology of the prepared materials in greater detail (Fig. 2). The raw clay (Fig. 2a) displays the typical lamellar structure

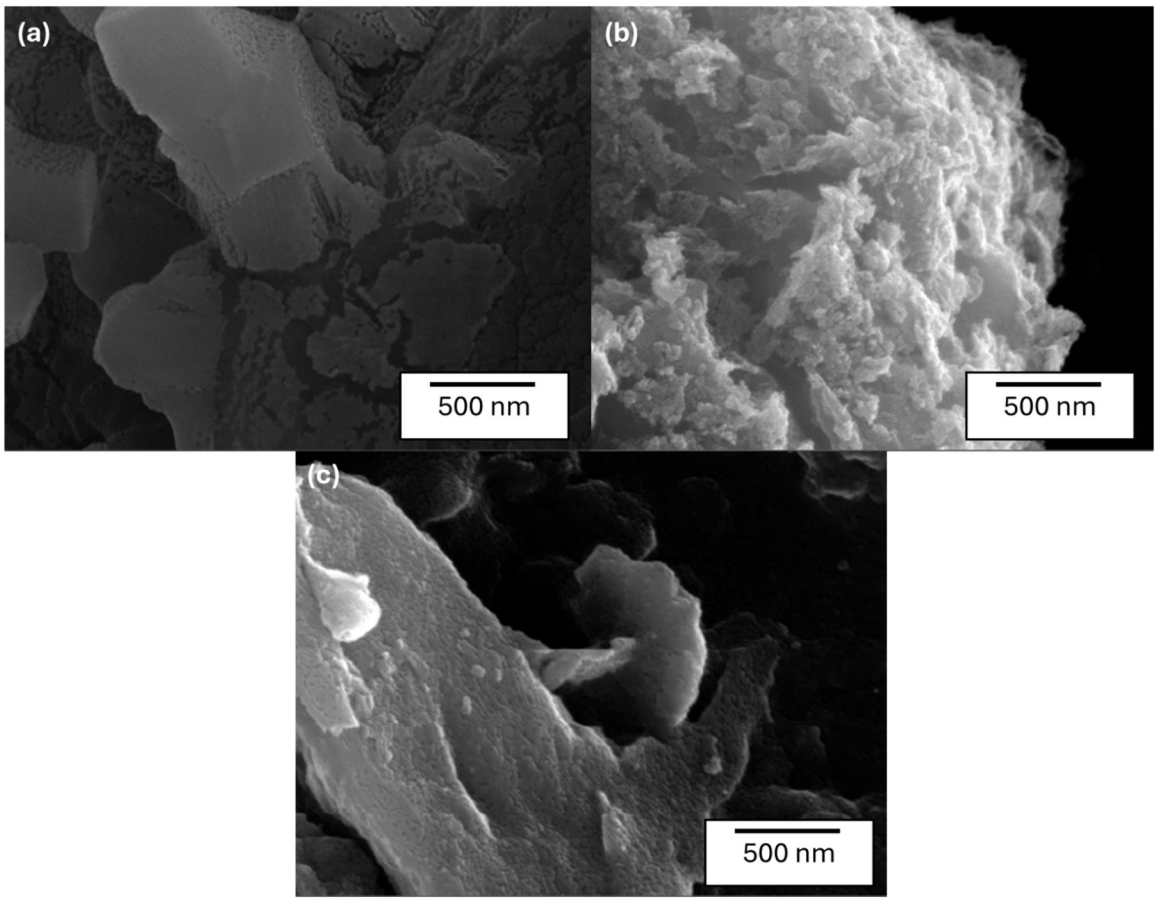

Fig. 2. SEM micrographs of (a) raw clay, (b) A/ZnO and (c) A/TiO_2 samples.

characteristic of montmorillonite-type clays, with stacked and slightly curved platelet-like layers. However, significant morphological transformations are observed after the sol-gel deposition of photocatalysts.

In both A/ZnO (Fig. 2b) and A/TiO_2 (Fig. 2c) samples, the clay surfaces appear to be homogeneously covered with granular particles, leading to a distinctly rougher and more textured surface. These particles correspond to ZnO or TiO_2 crystallites successfully deposited onto the clay layers. The absence of large aggregates and the relatively uniform distribution of the particles suggest an effective dispersion of the photocatalyst phase within the clay matrix.

This morphological evolution is consistent with the increase in specific surface area observed in the BET results (Table 2), particularly for A/TiO_2, which exhibits a highly porous structure. The intimate contact between the photocatalyst particles and the clay support is expected to enhance interfacial charge transfer and reduce recombination of photogenerated electron–hole pairs during photocatalytic processes.

Furthermore, the microstructural features observed by SEM support the role of the clay as a dispersing scaffold, preventing photocatalyst agglomeration and promoting a higher density of accessible active sites. This structural synergy between the clay and the metal oxide phase likely contributes to the improved photocatalytic and antibacterial performances observed in subsequent experiments.

3.3. Zeta potential and surface charge

Zeta potential measurements (Table 2) provide valuable insight into the surface charge properties and colloidal stability of the materials in aqueous suspension. These characteristics are crucial in governing particle aggregation, photocatalytic behavior, and interactions with charged pollutants or microbial membranes.

The raw clay exhibited a moderately negative zeta potential of –10.94 mV at pH 5.4, reflecting the natural surface charge of aluminosilicate layers due to isomorphic substitution and edge hydroxyl group ionization. Upon deposition of ZnO onto the clay (A/ZnO), a shift toward a slightly positive zeta potential (2.20 mV at pH 5.3) was observed. This indicates a successful surface modification and partial masking of the native clay charge by ZnO nanoparticles, which are typically amphoteric in character.

The ion-modified ZnO composites (A-Cu/ZnO, A-Na/ZnO, A-Zn/ZnO) all displayed increasingly positive zeta potentials, with values exceeding + 12 mV. This substantial shift confirms that the surface is dominated by the basic character of ZnO and/or the inserted metal ions. These positively charged surfaces may favor the adsorption of negatively charged pharmaceutical contaminants such as ibuprofen (predominantly anionic at neutral pH), as well as promote antibacterial effects through electrostatic interactions with bacterial cell walls.

Conversely, the TiO_2-based composites showed more variable zeta potential values, depending on the inserted ion. The undoped A/TiO_2 composite exhibited a mildly positive zeta potential (+2.50 mV at pH 3.2), whereas the Cu- and Zn-modified samples (A-Cu/TiO_2 and A-Zn/TiO_2) showed slightly negative values (–3.27 and –4.15 mV, respectively). Interestingly, A-Na/TiO_2 had a strongly negative zeta potential (–12.99 mV), even more so than the raw clay. This suggests that sodium ions enhance surface deprotonation or favor a more hydrated, negatively charged layer at the interface. Such surfaces may be less prone to aggregation but could exhibit reduced affinity for anionic molecules.

The point of zero charge (PZC) values, determined by electrokinetic measurements, further support these observations. ZnO-based composites showed PZCs ranging from 5.2 to 7.4, depending on the dopant, while TiO_2-based materials had lower PZCs (3.1–4.3), consistent with

their more acidic surface characteristics. Notably, A-Cu/ZnO and A-Na/ZnO had PZCs well above neutral pH, suggesting a strongly basic character, whereas A-Na/TiO_2 and A-Cu/TiO_2 had PZCs around 3.1–4.1, making them negatively charged under environmental pH conditions.

These findings demonstrate that the surface charge of the composites can be finely tuned by both the nature of the photocatalyst and the inserted cations. This tunability is key for optimizing adsorption and photocatalytic efficiency toward charged pharmaceutical compounds and for enhancing bactericidal action via electrostatic mechanisms.

3.4. Ibuprofen degradation

The photocatalytic activity of the synthesized materials was evaluated by monitoring the degradation of ibuprofen under UVA and UV-Vis irradiation, with results presented in Fig. 3. All experiments were performed in triplicate using a total catalyst concentration of 1 g/L, and mineralization was assessed via total organic carbon (TOC) analysis. Only ZnO and TiO_2 samples were also evaluated at 0.3 g/L. The kinetic study of IBU degradation under UVA light with A/ZnO and A-Cu/TiO_2 composite samples is shown in Fig. 4.

The raw clay exhibited no photocatalytic activity under either light condition, as expected due to the absence of photoactive components. In contrast, all composite materials demonstrated some degree of ibuprofen degradation, highlighting the contribution of the embedded photocatalyst phase.

Among the ZnO-based samples (Fig. 3), the pure ZnO reference (1 g/L) reached a maximum degradation efficiency of 30 % under both UVA and UV-Vis, whereas the A/ZnO composite reached 23 % under UVA and 10 % under UV-Vis. The lower activity of the A/ZnO composite relative to pure ZnO may be attributed to a partial coverage of active sites by the clay matrix or to reduced light absorption due to increased scattering. Additionally, ion-modified ZnO composites (A-Cu/ZnO, A-Na/ZnO, A-Zn/ZnO) exhibited significantly lower activities (8–10 %), suggesting that metal ion insertion may hinder charge separation or promote charge carrier recombination.

TiO_2-based materials exhibited overall superior performance (Fig. 3). The pure TiO_2 (1 g/L) achieved 45 % and 50 % degradation under UVA and UV-Vis, respectively. Notably, the A/TiO_2 composite also displayed high degradation rates, reaching 40 % under UVA and 35 % under UV-Vis, confirming efficient photocatalyst dispersion within the clay matrix.

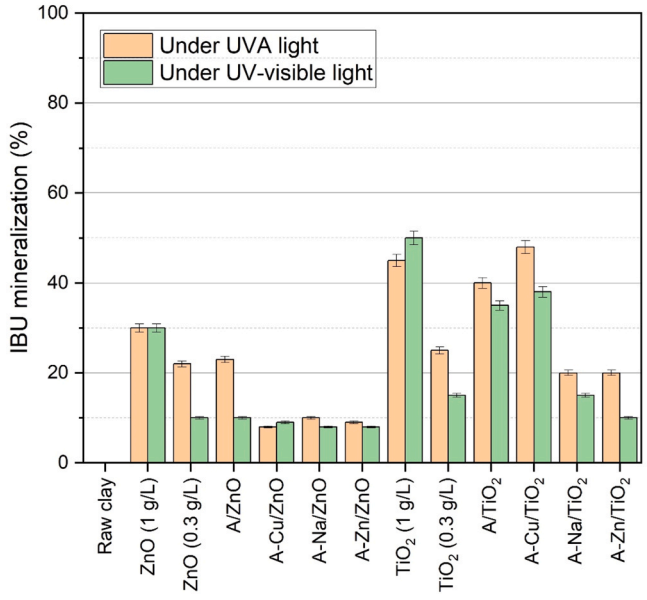

Fig. 3. Ibuprofen mineralization under UVA or UV–visible light after 4 h of illumination.

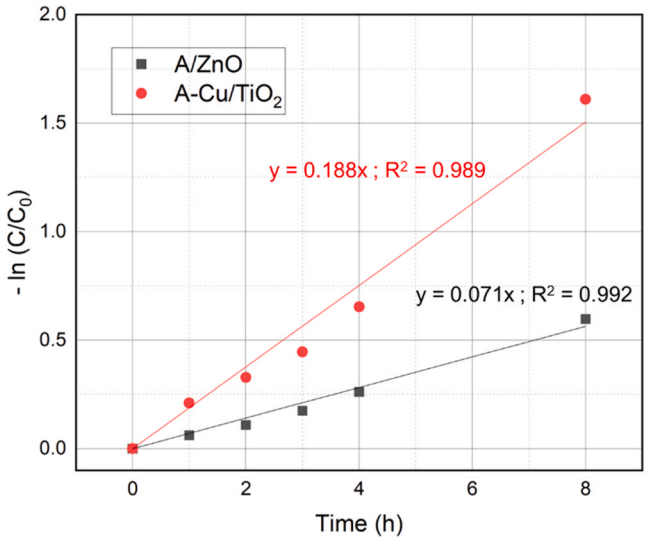

Fig. 4. Experimental determination of kinetic constant of IBU degradation for A/ZnO (black) and A-Cu/TiO_2 (red) samples under UVA light.

Among the doped TiO_2 composites, A-Cu/TiO_2 outperformed all others under UVA (48 %), while its performance dropped under UV-Vis (22 %), possibly due to limited visible-light absorption or dopant-induced recombination sites. In contrast, A-Na/TiO_2 and A-Zn/TiO_2 showed moderate activities (20 % or less), in line with their lower surface areas and less favorable textural and surface charge characteristics.

To better assess the intrinsic activity of the composites, control experiments were conducted using pure ZnO and TiO_2 at a lower dosage of 0.3 g/L, corresponding to the actual photocatalyst content in the composites (30 wt% in 1 g/L of material, as confirmed by ICP-AES, Table 1). Under these conditions, the degradation efficiency of ZnO decreased to 22 % (UVA) and 10 % (UV-Vis), closely matching that of A/ZnO. Similarly, TiO_2 at 0.3 g/L showed reduced degradation efficiencies (25 % UVA, 15 % UV-Vis), while A/TiO_2 still achieved significantly higher performance (40 % and 35 %, respectively).

These results clearly underline the beneficial role of the clay matrix in enhancing the effective utilization of the photocatalyst. The composite architecture, particularly in the case of A/TiO_2, appears to facilitate better dispersion of active sites, limit particle aggregation, and improve pollutant–catalyst interactions, leading to higher photocatalytic efficiency per unit mass of active material. Such features make these hybrid materials promising candidates for cost-effective water treatment applications where minimizing photocatalyst dosage is essential.

Fig. 4 shows that the kinetics of IBU degradation under UVA light are first order as the fitted curve of -ln(C/C_0) vs. time being linear for the 2 best composite samples, as previously observed in [40,41]. The kinetic constants can be calculated for each sample and are the slopes of the fitted curves in Fig. 4. The sample with the highest degradation (A-Cu/TiO_2) has the highest kinetic constant (Fig. 4).

To elucidate the reactive species involved in ibuprofen (IBU) degradation, scavenger experiments were conducted using the two most effective composite photocatalysts, A/ZnO and A-Cu/TiO_2, under UVA irradiation (1.2 mW/cm^2) for 4 h. The results, presented in Fig. 5, compare IBU degradation with and without the addition of three scavengers: ammonium oxalate (AO) for holes (h^+), isopropanol (ISOP) for hydroxyl radicals (•OH), and p-benzoquinone (PB) for superoxide radicals (O_2^-•). For both samples, the degradation trends were consistent. The addition of AO significantly reduced IBU degradation (by ~70–80 % based on preliminary data), as it scavenges photogenerated holes, thereby inhibiting the formation of •OH radicals via water oxidation, a key pathway in the process. Similarly, ISOP led to a

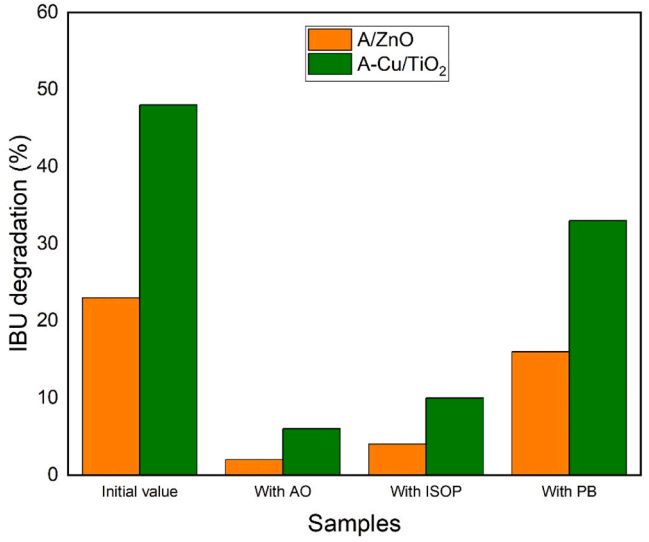

Fig. 5. IBU degradation with and without scavengers during 4 h under UVA light for (orange) A/ZnO and (green) A-Cu/TiO_2 samples. AO = ammonium oxalate, ISOP = isopropanol, PB = p-benzoquinone.

comparable decrease (~65–75 %), confirming the dominant role of •OH in IBU breakdown, consistent with the upstream inhibition observed with AO. In contrast, PB induced a moderate reduction (~20–30 %), suggesting that O_2^{-}• contributes less significantly to the degradation mechanism. These findings align with previous studies on photocatalytic systems, where hydroxyl radicals and holes were identified as the primary species for IBU degradation [40,42].

Metal leaching, particularly of zinc from ZnO-doped composites, is a critical factor to consider during photocatalytic degradation to prevent secondary pollution. In this study, ICP-AES analysis after 4 h under UVA (Table 3) revealed leaching levels of < 0.01 mg/L for Ti (TiO_2, A-Cu/TiO_2), 4 mg/L for Zn (ZnO), 0.1 mg/L for Zn (A/ZnO), and < 0.01 mg/L for Cu (A-Cu/TiO_2), indicating significant Zn release from unsupported ZnO compared to clay-supported A/ZnO, where leaching was reduced by 40-fold. These values remain below the WHO guideline of 3 mg/L for drinking water [47], suggesting acceptable environmental safety under tested conditions. Compared to Rahman et al. [48], who reported low copper leaching (<3 mg/L) with good reusability over five cycles in Fenton-like catalysts for ibuprofen degradation, our clay-supported composites demonstrate enhanced stability, particularly A/ZnO. However, the high Zn leaching from ZnO (4 mg/L) highlights the need for further optimization. Future studies should include extended cycle testing and ICP monitoring to ensure long-term stability and compliance with stricter environmental standards.

3.5. Bacteriological assay

The antibacterial properties of the synthesized materials were evaluated against several indicator microorganisms, including total coliforms, faecal coliforms, Escherichia coli, Salmonella/Shigella, and faecal streptococci. The tests were carried out using two complementary approaches: (i) culture on selective differential agars (XLD, Endo, and BEA) to monitor inhibition or reduction of target bacterial colonies, and (ii) a dilution-based viability assay on Mueller Hinton agar with various catalyst dosages (0.5, 1, and 10 g/L) to assess dose-dependent bactericidal effects. All tests were conducted under identical incubation conditions (37 °C, 24–48 h) and colony counts were expressed in log(CFU/mL).

Table 3
– ICP-AES measurement of metal leaching content after the photocatalytic experiment under UVA (4 h).

Samples	[Ti] after 4 h under UVA (mg/L)	[Zn] after 4 h under UVA (mg/L)	[Cu] after 4 h under UVA (mg/L)
TiO_2	< 0.01	-	-
A-Cu/TiO_2	< 0.01	-	< 0.01
ZnO	-	4	-
A/ZnO	-	0.1	-

- = not present in the sample initially

Control experiments were performed in the dark (with the materials, called Dark control in Fig. 6), under UVA alone (without materials, called Light control) and in the dark without the materials, all these conditions showed no reduction in bacteria populations. Light control and dark control without materials are not represented in Fig. 6 to avoid overloading it.

As shown in Fig. 6a, A/ZnO and A/TiO_2 composites led to a drastic reduction in the population of total and faecal coliforms, including E. coli, with complete inhibition observed at 1 g/L and above. This bactericidal effect was confirmed for enteric pathogens such as Salmonella and Shigella (Fig. 6b), as well as for Gram-positive faecal streptococci (Fig. 6c), demonstrating the broad-spectrum antimicrobial activity of these hybrid materials.

The raw clay already exhibited some antibacterial activity, especially against Salmonella/Shigella and faecal streptococci (Figs. 6b and 6c), while the ion-modified composites (A-Cu/ZnO, A-Na/ZnO, A-Zn/ZnO, and their TiO_2 analogues) showed moderate activity, generally requiring 10 g/L to achieve a significant reduction in CFU counts. This suggests that ion exchange alone is insufficient to induce bactericidal effects, and that the photocatalyst plays a central role. The bacterial activity of the raw clay suggests that the presence of ions in the raw clay (Table 1) can already inhibit the bacteria.

The strong antibacterial performance of A/ZnO and A/TiO_2, observed consistently across all tested strains and confirmed in Figs. 6a–6c, is likely related to the generation of reactive oxygen species (ROS) at the catalyst surface. These ROS, including hydroxyl radicals and superoxide anions, are known to damage bacterial membranes, proteins, and DNA [49,50]. Moreover, the surface charge of the composites may facilitate electrostatic interactions with negatively charged bacterial membranes, enhancing particle adhesion and subsequent membrane disruption.

Overall, these findings indicate that the developed hybrid materials, particularly A/ZnO and A/TiO_2, possess potent antibacterial activity, which complements their photocatalytic capabilities. This dual functionality is particularly advantageous for water treatment applications targeting both chemical micropollutants and microbial contamination.

3.6. From Material Design to Environmental Performance: A Comparative Perspective

The structure–function analysis of our hybrid materials reveals clear relationships between their physicochemical properties, such as specific surface area, zeta potential, and morphology, and their functional performance, including photocatalytic activity and antibacterial efficacy. These findings are consistent with recent literature on clay–photocatalyst composites.

Specific surface area plays a crucial role in pollutant degradation and antibacterial activity. For instance, the A/TiO_2 composite exhibits an exceptionally high specific surface area (325 m^2/g), while A/ZnO shows a respectable value (~125 m^2/g). These characteristics promote catalyst dispersion and access to active sites, as demonstrated by Adesina et al. [27], who reported approximately 84 % tetracycline removal after 2 h of exposure under UV and natural light with a kaolin–TiO_2–orange-peel biochar composite, attributing the performance to enhanced porosity and improved photocatalyst dispersion. Similarly, Yuan et al. [51] described montmorillonite/TiO_2 composites containing 30 wt% TiO_2 that achieved nearly complete dye degradation, correlating performance with superior dispersion and surface properties.

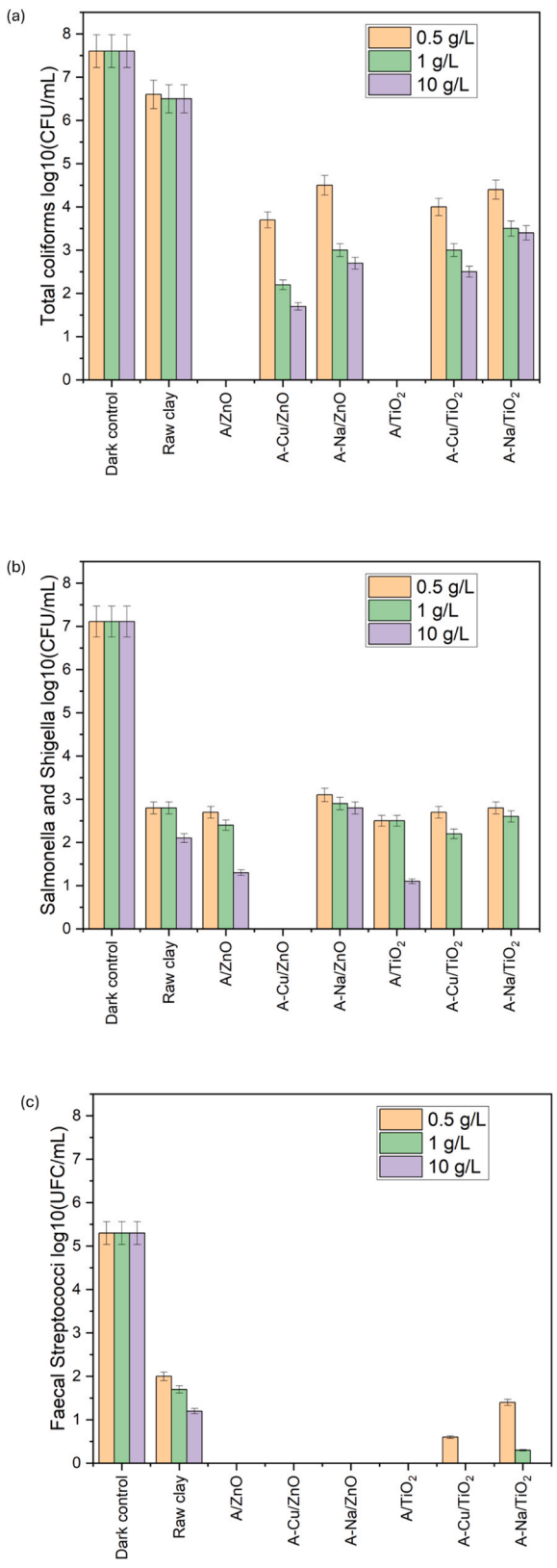

Fig. 6. Antibacterial activity on (a) total coliforms, (b) Salmonella/Shigella; and (c) faecal Strepotococci from the real wastewater. Previous to bacterial development the wastewater was stirred with the different samples under UVA illumination for 4 h. Light control and dark control without materials show no effect on any of the three bacteria (as Dark control) and so, are not represented on the figures to avoid overloading it.

Zeta potential is another key factor influencing pollutant adsorption and microbial interactions at the composite surface. Our ZnO-based composites acquire positive surface charge (up to +12 mV), favouring electrostatic attraction toward anionic contaminants, whereas TiO_2 variants have slightly negative to neutral charges, aligning with their distinct photoreactivity. Bai et al. [52] emphasized in their review that modulation of the zeta potential of clay-supported TiO_2/ZnO photocatalysts enhances affinity for anionic contaminants and improves photocatalytic efficiency.

When normalized to active-phase mass, our A/TiO_2 composites clearly outperform pure TiO_2 at equivalent loadings, highlighting the benefits of clay-supported systems. These results align with those of Karchiyappan et al. [53], who demonstrated that kaolin/TiO_2 composites synthesized via sol–gel methods deliver higher photocatalytic removal rates than pure TiO_2. Additionally, pillared montmorillonite (Ti-PILC) structures exhibit improved surface area and stability, further enhancing performance compared to unmodified oxide powders [28].

Regarding antibacterial activity, our A/ZnO and A/TiO_2 composites produced near-complete bacterial inhibition at concentrations $\geq$ 1 g/L. Wu et al. [50] reported similar outcomes for montmorillonite–Ag/TiO_2 composites under visible light, attributing bactericidal efficacy to reactive oxygen species (ROS)-induced membrane damage. Li et al. [49] also achieved remarkable antibacterial and pharmaceutical degradation performance using a kaolinite–TiO_2–g-C_3N_4 heterojunction, confirming the synergy between clay support and photocatalyst.

Overall, our hybrid materials offer performance comparable or superior to other clay–photocatalyst systems reported in the literature for dye removal, micropollutant degradation, or microbial decontamination. For example, orange-peel biochar/clay/TiO_2 composites demonstrated 89–92 % tetracycline degradation with 50 % of mineralization under UVB for 2 h and efficient E. coli inactivation without forming toxic intermediates [27]. In that study, the illumination was much more energetic than the present work. Similarly, a 3D-printed ZnO/clay architecture showed effective methylene blue degradation with 100 % degradation in 40 min under solar irradiation [54] but no mineralization was assessed.

Concerning the photocatalytic mineralization of ibuprofen, our study demonstrates a compelling 48 % Total Organic Carbon (TOC) reduction within 4 h using the A-Cu/TiO_2 composite under UVA irradiation with low intensity (1.2 mW/cm^2) [55], surpassing several literature benchmarks in terms of efficiency, practicality, and multifunctionality. For instance, Tanveer et al. [56] achieved 47 % TOC removal with UV/ZnO after only 15 min but required artificial UVC lamps (254 nm) and showed lower performance under solar conditions with quartz or borosilicate reactors, highlighting the limitations of non-supported catalysts in real-world applications, while at catalyst dosing of 1.5 g/L TiO_2 and 0.5 g/L ZnO, degradation rates were similar, with UV lamp-based photocatalysis yielding higher TOC and COD reduction than solar irradiation. Similarly, Loaiza-Ambuludi et al. [57] reported up to 90 % TOC abatement via UVC/H_2O_2/Fe photo-Fenton after 8 h, yet this homogeneous process necessitates high oxidant doses and lacks the catalyst recovery ease offered by our clay-supported system, with pseudo-second-order kinetics observed for TOC decay. Mendez-Arriaga et al. [58] attained 80 % Dissolved Organic Carbon (DOC) removal in 240 min through sonophoto-Fenton/TiO_2 hybrids under UV-Vis or visible light, but relied on energy-intensive ultrasound and extended reaction times without integrating antimicrobial properties, achieving up to 90 % mineralization with US/UV/TiO_2/H_2O_2/Fe. Jimenez-Salcedo et al. [59] focused on degradation pathways using TiO_2/UV and g-C_3N_4/visible light, identifying intermediates like 2-(4-acrylphenyl) acetic acid and 4-propenylbenzoic acid but not quantifying mineralization, highlighting incomplete breakdown and potential toxicity persistence absent in our approach, with degradation efficiencies varying by pH and light intensity. More recently, Pylarinou et al. [60] achieved efficient ibuprofen degradation with TiO_2/Mo-$BiVO_4$ bilayers under photoelectrocatalysis, yielding photocurrent densities up to

0.5 mA/cm^2 and 90 % removal in 120 min, yet mineralization data were not emphasized, and the complex electrode fabrication contrasts with our low-cost, natural smectite-derived composites. Across these studies and others, such as Braz et al. [61] with 50 % mineralization using pure TiO_2 under UV after 60 min, Candido et al. [33] reporting up to 78 % TOC reduction with TiO_2 in 60 min under UV lamp, Gong et al. [62] achieved higher mineralization rates (up to 60 % in 20 min) with a Fe^{2+}/Oxone/UV process, but required higher oxidant doses and showed toxicity evolution, and Feng et al. [63] using YMO-SO photocatalysts, reached 70–80 % degradation under visible light but reported lower mineralization (typically <40 % TOC removal) and relied on complex synthesis methods, typical mineralization ranges from 20 % to 80 % over 2–6 h with photocatalytic systems, often facing recovery challenges and higher costs.

Direct comparison between these studies is challenging due to significant variations in experimental conditions, such as the type and intensity of illumination (e.g., UVA vs. UVC lamps or solar simulators), pollutant and catalyst concentrations, and irradiation durations, which can range from 120 to 360 min across different setups. Moreover, not all articles provide comprehensive details on these parameters, including precise light power outputs or exact catalyst loadings, making quantitative benchmarking challenging. Despite these inconsistencies, our A-Cu/TiO_2 system stands out for its balanced efficiency under practical UVA conditions, highlighting its potential for scalable applications.

3.7. Limitations of this work

Despite the promising results, this study presents several limitations that warrant consideration. First, the photocatalytic performance under visible light remains suboptimal, with lower degradation rates compared to UVA conditions, indicating a need for further optimization to enhance visible-light responsiveness. Second, the long-term stability and reusability of the clay-supported composites were not fully assessed, as tests were limited to some cycles, potentially underestimating material degradation or leaching over extended use but giving first promising results. Third, the experiments were conducted under controlled laboratory conditions, which may not fully replicate the complex matrix of real wastewater, including varying pH, competing pollutants, and microbial loads. Finally, the scalability of the synthesis process and its economic viability in resource-limited settings require further investigation to ensure practical implementation in decentralized treatment systems.

4. Conclusion

In this study, a series of clay-based photocatalytic composites incorporating ZnO or TiO_2, with or without additional ion exchange (Cu, Na, Zn), were successfully synthesized and characterized. Elemental analysis and XRD confirmed the effective incorporation of photocatalyst phases without significant alteration of either their crystalline structure or clay matrix. Textural analysis revealed a substantial influence of both the photocatalyst type and the exchanged cations on surface area, porosity, and particle dispersion. TiO_2-based materials generally exhibited higher surface areas and more favorable morphologies than their ZnO-based counterparts, especially in undoped configurations.

Zeta potential and point of zero charge analyses showed that the surface charge of the composites could be finely tuned via cationic modification, influencing their colloidal stability and potential interaction with charged pollutants or microbial membranes. SEM imaging further confirmed the homogeneous dispersion of photocatalyst particles on the clay surface, contributing to the accessible active surface.

Photocatalytic degradation tests using ibuprofen as a model contaminant demonstrated that all composites exhibited measurable activity under UVA and UV-Vis irradiation, with TiO_2-based composites showing superior performance overall. Among these, the Cu-doped TiO_2 sample (A-Cu/TiO_2) achieved the highest degradation under UVA, suggesting a synergistic effect between copper doping and the clay support. However, performance under visible light was generally lower, indicating room for improvement in enhancing visible-light responsiveness.

Overall, the results highlight the potential of these hybrid materials as efficient and tunable photocatalytic platforms for water treatment applications. The structural, textural, and surface properties can be adjusted by choice of photocatalyst and exchanged ions, enabling the rational design of multifunctional materials for both pollutant degradation and antimicrobial applications. Future work will focus on optimizing the photocatalyst loading, improving visible-light activity, and assessing long-term stability and regeneration potential in real water matrices.

CRediT authorship contribution statement

Marlène Huguette Tsaffo Mbognou: Conceptualization, Writing – review & editing, Investigation, Formal analysis. **Stéphanie D. Lambert:** Conceptualization, Methodology, Writing – review & editing, Funding acquisition, Project administration. **Antoine Farcy:** Investigation, Formal analysis, Writing – review & editing. **Hela Rekik:** Investigation, Formal analysis, Writing – review & editing. **Steven C. N. Wouamba:** Investigation, Formal analysis, Writing – review & editing. **Emmanuel Djoufac Woumfo:** Supervision, Funding acquisition, Project administration, Writing – review & editing. **Julien G. Mahy:** Conceptualization, Methodology, Writing – original draft, Writing – review & editing, Investigation, Supervision, Formal analysis, Validation.

Declaration of Competing Interest

The authors declare that they have no known competing financial interests or personal relationships that could have appeared to influence the work reported in this paper.

Acknowledgements

Marlène Huguette Tsaffo Mbognou thanks the PACODEL for a doctoral grant. Stéphanie D. Lambert thanks the F.R.S.-FNRS for her Research Director position. The authors thank the CARPORVISU platform of the University of Liège and its manager, Dr. Alexandre Léonard, for the nitrogen adsorption–desorption measurements. The authors thank Bruno Correia for his carefully reading and corrections of the paper.

Data Availability

The raw/processed data required to reproduce these findings can be shared on demand.

References

[1] A.S. Adeleye, J. Xue, Y. Zhao, A.A. Taylor, J.E. Zenobio, Y. Sun, Z. Han, O. A. Salawu, Y. Zhu, Abundance, fate, and effects of pharmaceuticals and personal care products in aquatic environments, J. Hazard Mater. 424 (2022), https://doi.org/10.1016/j.jhazmat.2021.127284.

[2] M. Caban, E. Lis, J. Kumirska, P. Stepnowski, Determination of pharmaceutical residues in drinking water in Poland using a new SPE-GC-MS(SIM) method based on speedisk extraction disks and DIMETRIS derivatization, Sci. Total Environ. 538 (2015) 402–411, https://doi.org/10.1016/j.scitotenv.2015.08.076.

[3] G.R.K. Kenmogne, F. Rosillon, H.G. Mpakam, A. Nono, Enjeux sanitaires, socio-économiques et environnementaux liés à la réutilisation des eaux usées dans le maraîchage urbain: cas du bassin versant de l'Abiergué (Yaoundé-Cameroun), VertigOLa Rev. Électron. En. Sci. De. l'Environ. (2010).

[4] Organisation mondiale de la santé, NOTE D'ORIENTATION TECHNIQUE RELATIVE À L'EAU, L'ASSAINISSEMENT ET L'HYGIÈNE ET LA GESTION DES EAUX USÉES POUR PRÉVENIR LES INFECTIONS ET RÉDUIRE LA PROPAGATION DE LA RÉSISTANCE AUX ANTIMICROBIENS, 2020. ⟨https://iris.who.int/bitstream/handle/10665/336678/9789240014831-fre.pdf⟩ (accessed June 17, 2025).

[5] N. Walczak, A. Krzyszczak-Turczyn, B. Czech, Unveiling the effect of SWCNT as the dopants of TiO2 in pharmaceutical mixture photocatalytic removal from water and wastewater, J. Photochem. Photobio. A Chem. 467 (2025), https://doi.org/10.1016/j.jphotochem.2025.116437.
[6] N. Dammak, N. Fakhfakh, S. Fourmentin, M. Benzina, Natural clay as raw and modified material for efficient o-xylene abatement, J. Environ. Chem. Eng. 1 (2013) 667–675, https://doi.org/10.1016/j.jece.2013.07.001.
[7] M.R. Eskandarian, H. Choi, M. Fazli, M.H. Rasoulifard, Effect of UV-LED wavelengths on direct photolytic and TiO2 photocatalytic degradation of emerging contaminants in water, Chem. Eng. J. 300 (2016) 414–422, https://doi.org/10.1016/j.cej.2016.05.049.
[8] D.S. Villarreal-Lucio, V.S. Galván-Romero, C. López-Saldaña, B.V. Loera-García, K. X. Vargas-Berrones, R. Ocampo-Pérez, J.C. Serna-Carrizalez, R. Flores-Ramírez, Molecularly imprinted polymer with photocatalytic activity for ibuprofen adsorption, degradation, and detection in real water samples, J. Contam. Hydrol. 273 (2025), https://doi.org/10.1016/j.jconhyd.2025.104600.
[9] M. Gros, M. Petrović, A. Ginebreda, D. Barceló, Removal of pharmaceuticals during wastewater treatment and environmental risk assessment using hazard indexes, Environ. Int 36 (2010) 15–26, https://doi.org/10.1016/j.envint.2009.09.002.
[10] N. Bashir, T. Sawaira, A. Jamil, M. Awais, A. Habib, A. Afzal, Challenges and prospects of main-group metal-doped TiO2 photocatalysts for sustainable water remediation, Mater. Today Sustain. 27 (2024), https://doi.org/10.1016/j.mtsust.2024.100869.
[11] M.I. Din, R. Khalid, Photocatalysis of pharmaceuticals and organic dyes in the presence of silver-doped TiO2 photocatalyst–a critical review, Int J. Environ. Anal. Chem. 105 (2025) 276–300, https://doi.org/10.1080/03067319.2023.2258795.
[12] S. Douven, J.G. Mahy, C. Wolfs, C. Reyserhove, D. Poelman, F. Devred, E. M. Gaigneaux, S.D. Lambert, Efficient N, fe Co-Doped TiO2 active under Cost-Effective visible LED light: from powders to films, Catalysts 10 (2020) 547, https://doi.org/10.3390/catal10050547.
[13] J.G. Mahy, M.H.T. Mbognou, C. Léonard, N. Fagel, E.D. Woumfo, S.D. Lambert, Natural clay modified with ZnO/TiO2 to enhance pollutant removal from water, Catalysts 12 (2022), https://doi.org/10.3390/catal12020148.
[14] J.G. Mahy, C. Wolfs, C. Vreuls, S. Drot, S. Dircks, A. Boergers, J. Tuerk, S. Hermans, S.D. Lambert, Advanced oxidation processes for waste water treatment: from lab-scale model water to on-site real waste water, Environ. Technol. 42 (2021) 3974–3986, https://doi.org/10.1080/09593330.2020.1797894.
[15] H. Benhebal, C. Wolfs, S. Kadi, R.G. Tilkin, B. Allouche, D. Lambert, J.G. Mahy, Visible light sensitive SnO2/ZnCo2O4 material for the photocatalytic removal of organic pollutants in water, Inorganics 7 (2019) 77.
[16] P. Trigueiro, A.G. Jerônimo, W.A. Albuquerque, W.L. da Silva, J.A. Osajima, M. Jaber, R.R. Peña-Garcia, Shaping a ZnO-alginate-hectorite nanocomposite for improved photocatalytic drug removal, Appl. Mater. Today 44 (2025), https://doi.org/10.1016/j.apmt.2025.102680.
[17] P. Trigueiro, W.A. Albuquerque, A.G. Jerônimo, R. Barbosa, M. Jaber, R.R. Peña-Garcia, Tailoring Y-doped ZnO loaded onto eco-friendly support alginate-hectorite for azo dye removal, Appl. Surf. Sci. 704 (2025), https://doi.org/10.1016/j.apsusc.2025.163461.
[18] W. Albuquerque, P. Trigueiro, B.V. Silva, L. Neves, L.C. Almeida, R.R. Peña-Garcia, A novel RuO_2@ZnO-Alginate-Halloysite composite for the effective degradation of eosin yellow dye and ciprofloxacin drug, Mater. Res Bull. 182 (2025), https://doi.org/10.1016/j.materresbull.2024.113178.
[19] P. Trigueiro, W.A. Albuquerque, A.G. Jerônimo, M.S. Rodrigues, E.L.T. França, R. R. Peña-Garcia, CuO-TiO2–Saponite ternary nanocomposite for efficient removal of bromocresol Green dye, Minerals 14 (2024), https://doi.org/10.3390/min14121268.
[20] R.P. Feitosa, I.S. de Lima, Y. Guerra, E.C. da Silva-Filho, M.B. Furtini, L. Almeida, R.R. Peña-Garcia, I.B. Martín, J.A. Cecília, J.A. Osajima, Cerium-Doped TiO2 and sepiolite nanocomposites for tetracycline inactivation in water treatment, ACS Appl. Nano Mater. 8 (2025) 4324–4338, https://doi.org/10.1021/acsanm.4c01068.
[21] R.F. Hamarawf, D.I. Tofiq, K.H.H. Aziz, H.Q. Hassan, K.A. Abdalkarim, S. J. Mohammed, Antibacterial activity and photo-Fenton catalytic degradation of a novel FeII/FeIII mixed-valency porous coordination polymer, J. Environ. Chem. Eng. 13 (2025), https://doi.org/10.1016/j.jece.2025.116765.
[22] K.H.H. Aziz, K.M. Omer, A. Mahyar, H. Miessner, S. Mueller, D. Moeller, Application of photocatalytic falling film reactor to elucidate the degradation pathways of pharmaceutical diclofenac and ibuprofen in aqueous solutions, Coatings 9 (2019), https://doi.org/10.3390/coatings9080465.
[23] A.S. Soares, F.P. Araujo, R. França, J.A. Osajima, Y. Guerra, S. Castro-Lopes, E. C. Silva-Filho, F.E. Santos, L.C. Almeida, B.C. Viana, R.R. Peña-Garcia, Effect of ph on the growth and ibuprofen photocatalytic response of Zn1 − xCoxO compound synthesized by the co-precipitation method, J. Mater. Res 38 (2023) 2439–2452, https://doi.org/10.1557/s43578-023-00980-4.
[24] J.G. Mahy, L. Lejeune, T. Haynes, N. Body, S. De Kreijger, B. Elias, R.H.M. Marcilli, C.A. Fustin, S. Hermans, Crystalline ZnO photocatalysts prepared at ambient temperature: influence of morphology on p-nitrophenol degradation in water, Catalysts 11 (2021), https://doi.org/10.3390/catal11101182.
[25] J.G. Mahy, C.A. Paez, J. Hollevoet, L. Courard, E. Boonen, S.D. Lambert, Durable photocatalytic thin coatings for road applications, Constr. Build. Mater. 215 (2019) 422–434, https://doi.org/10.1016/j.conbuildmat.2019.04.222.
[26] F. Méndez-Arriaga, S. Esplugas, J. Giménez, Photocatalytic degradation of non-steroidal anti-inflammatory drugs with TiO2 and simulated solar irradiation, Water Res 42 (2008) 585–594, https://doi.org/10.1016/j.watres.2007.08.002.
[27] M.O. Adesina, M.O. Alfred, H. Seitz, K. Brennenstuhl, H.M. Rawel, P. Wessig, J. Kim, A. Wedel, W. Koopman, C. Günter, E.I. Unuabonah, A. Taubert, Orange peel biochar/clay/titania composites: low cost, high performance, and easy-to-reuse photocatalysts for the degradation of tetracycline in water, Environ. Sci. 10 (2024) 1432–1450, https://doi.org/10.1039/d4ew00037d.
[28] M. Chauhan, V.K. Saini, S. Suthar, Ti-pillared montmorillonite clay for adsorptive removal of amoxicillin, imipramine, diclofenac-sodium, and paracetamol from water, J. Hazard Mater. 399 (2020), https://doi.org/10.1016/j.jhazmat.2020.122832.
[29] E.G. Garrido-Ramírez, B.K.G. Theng, M.L. Mora, Clays and oxide minerals as catalysts and nanocatalysts in Fenton-like reactions - a review, Appl. Clay Sci. 47 (2010) 182–192, https://doi.org/10.1016/j.clay.2009.11.044.
[30] H. Bel Hadjltaief, P. Da Costa, M.E. Galvez, M. Ben Zina, Influence of operational parameters in the heterogeneous photo-fenton discoloration of wastewaters in the presence of an iron-pillared clay, Ind. Eng. Chem. Res 52 (2013) 16656–16665, https://doi.org/10.1021/ie4018258.
[31] M.H.T. Mbognou, S.D. Lambert, J. Caucheteux, A. Farcy, C. Alié, N. Fagel, E. D. Woumfo, J.G. Mahy, Hybrid clay-based materials for organic dyes and pesticides elimination in water, J. Solgel Sci. Technol. 105 (2023) 461–470, https://doi.org/10.1007/s10971-022-06005-6.
[32] K.H. Hama Aziz, H. Miessner, S. Mueller, D. Kalass, D. Moeller, I. Khorshid, M.A. M. Rashid, Degradation of pharmaceutical diclofenac and ibuprofen in aqueous solution, a direct comparison of ozonation, photocatalysis, and non-thermal plasma, Chem. Eng. J. 313 (2017) 1033–1041, https://doi.org/10.1016/j.cej.2016.10.137.
[33] J.P. Candido, S.J. Andrade, A.L. Fonseca, F.S. Silva, M.R.A. Silva, M.M. Kondo, Ibuprofen removal by heterogeneous photocatalysis and ecotoxicological evaluation of the treated solutions, Environ. Sci. Pollut. Res. 23 (2016) 19911–19920, https://doi.org/10.1007/s11356-016-6947-z.
[34] H. Benhebal, M. Chaib, A. Leonard, S.D. Lambert, M. Crine, Photodegradation of phenol and benzoic acid by sol-gel-synthesized alkali metal-doped ZnO, Mater. Sci. Semicond. Process 15 (2012) 264–269, https://doi.org/10.1016/j.mssp.2011.12.001.
[35] J.G. Mahy, G.L.-M. Léonard, S. Pirard, D. Wicky, A. Daniel, C. Archambeau, D. Liquet, B. Heinrichs, Aqueous sol-gel synthesis and film deposition methods for the large-scale manufacture of coated steel with self-cleaning properties, J. Solgel Sci. Technol. 81 (2017) 27–35, https://doi.org/10.1007/s10971-016-4020-5.
[36] M. Schreier, J.R. Regalbuto, a fundamental study of pt tetraammine impregnation of silica: 1. The electrostatic nature of platinum adsorption, J. Catal. 225 (2004) 190–202, https://doi.org/10.1016/j.jcat.2004.03.034.
[37] V. Claude, J.G. Mahy, T. Lohay, R.G. Tilkin, F. Micheli, S.D. Lambert, Sol – gel synthesis of Ni/Al2O3 catalysts for toluene reforming: support modification with alkali, alkaline earth or rare-earth dopant (Ca,K,Mg or Ce), Surf. Interfaces 20 (2020) 100511, https://doi.org/10.1016/j.surfin.2020.100511.
[38] F.S. Mustafa, K.H. Hama Aziz, Heterogeneous catalytic activation of persulfate for the removal of rhodamine b and diclofenac pollutants from water using iron-impregnated biochar derived from the waste of black seed pomace, Process Saf. Environ. Prot. 170 (2023) 436–448, https://doi.org/10.1016/j.psep.2022.12.030.
[39] C.M. Malengreaux, G.M.-L. Léonard, S.L. Pirard, I. Cimieri, S.D. Lambert, J. R. Bartlett, B. Heinrichs, How to modify the photocatalytic activity of TiO2 thin films through their roughness by using additives. A relation between kinetics, morphology and synthesis, Chem. Eng. J. 243 (2014) 537–548, https://doi.org/10.1016/j.cej.2013.11.031.
[40] A.S. Sá, R.P. Feitosa, L. Honório, R. Peña-Garcia, L.C. Almeida, J.S. Dias, L. P. Brazuna, T.G. Tabuti, E.R. Triboni, J.A. Osajima, E.C. da Silva-Filho, A brief photocatalytic study of zno containing cerium towards ibuprofen degradation, Materials 14 (2021), https://doi.org/10.3390/ma14195891.
[41] N. Shafeei, G. Asadollahfardi, G. Moussavi, M.M.Akbar Boojar, Degradation of ibuprofen in the photocatalytic process with doped TiO 2 as catalyst and UVA-LED as existing source, Desalin. Water Treat. 142 (2019) 341–352, https://doi.org/10.5004/dwt.2019.23214.
[42] C.B. Anucha, I. Altin, E. Bacaksiz, I. Degirmencioglu, T. Kucukomeroglu, S. Yılmaz, V.N. Stathopoulos, Immobilized tio2/zno sensitized copper (Ii) phthalocyanine heterostructure for the degradation of ibuprofen under uv irradiation, Separations 8 (2021) 1–21, https://doi.org/10.3390/separations8030024.
[43] A. Farcy, M. Mathy, L. Lejeune, P. Eloy, S. Hermans, P. Drogui, J.G. Mahy, Ce2O3 and TiO2 p-n heterojunction for enhanced degradation of p-nitrophenol under visible light, J. Photochem. Photobio. A Chem. 463 (2025), https://doi.org/10.1016/j.jphotochem.2025.116284.
[44] H.B. Saab, N. Nassif, A.G. El Samrani, R. Daoud, S. Medawar, N. Ouaïni, Survey of bacteriological surface water quality (Nahr Ibrahin River, Lebanon), Rev. Des. Sci. De. l'Eau 20 (2007) 341–352, https://doi.org/10.7202/016909ar.
[45] G. Zerjav, K. Zizek, J. Zavasnik, A. Pintar, Brookite vs. Rutile vs. Anatase: What's behind their various photocatalytic activities? J. Environ. Chem. Eng. 10 (2022) https://doi.org/10.1016/j.jece.2022.107722.
[46] W.A. Freitas, B.E.C.F. Soares, M.S. Rodrigues, P. Trigueiro, L.M.C. Honorio, R. Peña-Garcia, A.C.S. Alcântara, E.C. Silva-Filho, M.G. Fonseca, M.B. Furtini, J. A. Osajima, Facile synthesis of ZnO-clay minerals composites using an ultrasonic approach for photocatalytic performance, J. Photochem. Photobio. A Chem. 429 (2022), https://doi.org/10.1016/j.jphotochem.2022.113934.
[47] World Health Organization (WHO), Guidelines for Drinking-water Quality FOURTH EDITION INCORPORATING THE FIRST ADDENDUM, Geneva, 2017.
[48] K.O. Rahman, K.H.H. Aziz, Utilizing scrap printed circuit boards to fabricate efficient Fenton-like catalysts for the removal of pharmaceutical diclofenac and ibuprofen from water, J. Environ. Chem. Eng. 10 (2022), https://doi.org/10.1016/j.jece.2022.109015.
[49] C. Li, Z. Sun, W. Zhang, C. Yu, S. Zheng, Highly efficient g-C3N4/TiO2/kaolinite composite with novel three-dimensional structure and enhanced visible light

responding ability towards ciprofloxacin and S. Aureus, Appl. Catal. B 220 (2018) 272–282, https://doi.org/10.1016/j.apcatb.2017.08.044.
[50] T.S. Wu, K.X. Wang, G.D. Li, S.Y. Sun, J. Sun, J.S. Chen, Montmorillonite-Supported Ag/TiO2 nanoparticles: an efficient visible-Light bacteria photodegradation material, ACS Appl. Mater. Interfaces 2 (2010) 544–550, https://doi.org/10.1021/am900743d.
[51] L. Yuan, D. Huang, W. Guo, Q. Yang, J. Yu, TiO2/montmorillonite nanocomposite for removal of organic pollutant, Appl. Clay Sci. 53 (2011) 272–278, https://doi.org/10.1016/j.clay.2011.03.013.
[52] N. Bai, X. Liu, Z. Li, X. Ke, K. Zhang, Q. Wu, High-efficiency TiO2/ZnO nanocomposites photocatalysts by sol–gel and hydrothermal methods, J. Solgel Sci. Technol. 99 (2021) 92–100, https://doi.org/10.1007/s10971-021-05552-8.
[53] T. Karchiyappan, R. Rao, K. Mohammad, H. Dehghani, Water science and technology library industrial wastewater treatment emerging technologies for sustainability, Springer, 2022. ⟨https://www.springer.com/gp/⟩.
[54] S. Ali, M.T. Aljarrah, A. Al-Otoom, N. Abdelaziz, Development and testing of robust 3D printed ZnO/Clay photocatalysts for sustainable wastewater treatment, ACS Omega (2025), https://doi.org/10.1021/acsomega.4c09879.
[55] K.M. Reza, A. Kurny, F. Gulshan, Parameters affecting the photocatalytic degradation of dyes using TiO2: a review, Appl. Water Sci. 7 (2017) 1569–1578, https://doi.org/10.1007/s13201-015-0367-y.
[56] M. Tanveer, G.T. Guyer, G. Abbas, Photocatalytic degradation of ibuprofen in water using TiO2 and ZnO under artificial UV and solar irradiation, Water Environ. Res. 91 (2019) 822–829, https://doi.org/10.1002/wer.1104.
[57] S. Loaiza-Ambuludi, M. Panizza, N. Oturan, M.A. Oturan, Removal of the anti-inflammatory drug ibuprofen from water using homogeneous photocatalysis, Catal. Today 224 (2014) 29–33, https://doi.org/10.1016/j.cattod.2013.12.018.
[58] F. Méndez-Arriaga, R.A. Torres-Palma, C. Pétrier, S. Esplugas, J. Gimenez, C. Pulgarin, Mineralization enhancement of a recalcitrant pharmaceutical pollutant in water by advanced oxidation hybrid processes, Water Res 43 (2009) 3984–3991, https://doi.org/10.1016/j.watres.2009.06.059.
[59] M. Jiménez-Salcedo, M. Monge, M.T. Tena, Photocatalytic degradation of ibuprofen in water using TiO2/UV and g-C3N4/visible light: study of intermediate degradation products by liquid chromatography coupled to high-resolution mass spectrometry, Chemosphere 215 (2019) 605–618, https://doi.org/10.1016/j.chemosphere.2018.10.053.
[60] M. Pylarinou, E. Sakellis, S. Gardelis, V. Psycharis, M.G. Kostakis, N.S. Thomaidis, V. Likodimos, Bilayer TiO2/Mo-BiVO4 photoelectrocatalysts for ibuprofen degradation, Materials 18 (2025), https://doi.org/10.3390/ma18020344.
[61] F.S. Braz, M.R.A. Silva, F.S. Silva, S.J. Andrade, A.L. Fonseca, M.M. Kondo, Photocatalytic degradation of ibuprofen using TiO₂ and ecotoxicological assessment of degradation intermediates against <I>Daphnia similis</I&gt, J. Environ. Prot. 05 (2014) 620–626, https://doi.org/10.4236/jep.2014.57063.
[62] H. Gong, W. Chu, S.H. Lam, A.Y.C. Lin, Ibuprofen degradation and toxicity evolution during Fe2+/Oxone/UV process, Chemosphere 167 (2017) 415–421, https://doi.org/10.1016/j.chemosphere.2016.10.027.
[63] Z. Feng, Synthesis and full-spectrum-responsive photocatalytic activity from UV/Vis to near-infrared region of S-O decorated YMnO3 nanoparticles for photocatalytic degradation of ibuprofen, Front Chem. 12 (2024), https://doi.org/10.3389/fchem.2024.1424548.